Supplemental Materials

Molecular Biology of the Cell

Gupta *et al*.

Supplementary Material for

Regulation of p65 nuclear localization and chromatin states by compressive force

Rajshikhar Gupta,[1,2] Paulina Schärer,[2] Yawen Liao,[1,2] Bibhas Roy,[2] Roger M. Benoit,[2] GV Shivashankar[1,2*]

[1]Department of Health Sciences and Technology, ETH Zürich, Zürich, Switzerland

[2]Laboratory of Nanoscale Biology, Paul Scherrer Institut, Villigen, Aargau, Switzerland

[*]To whom correspondence should be addressed; E-mail: gshivasha@ethz.ch

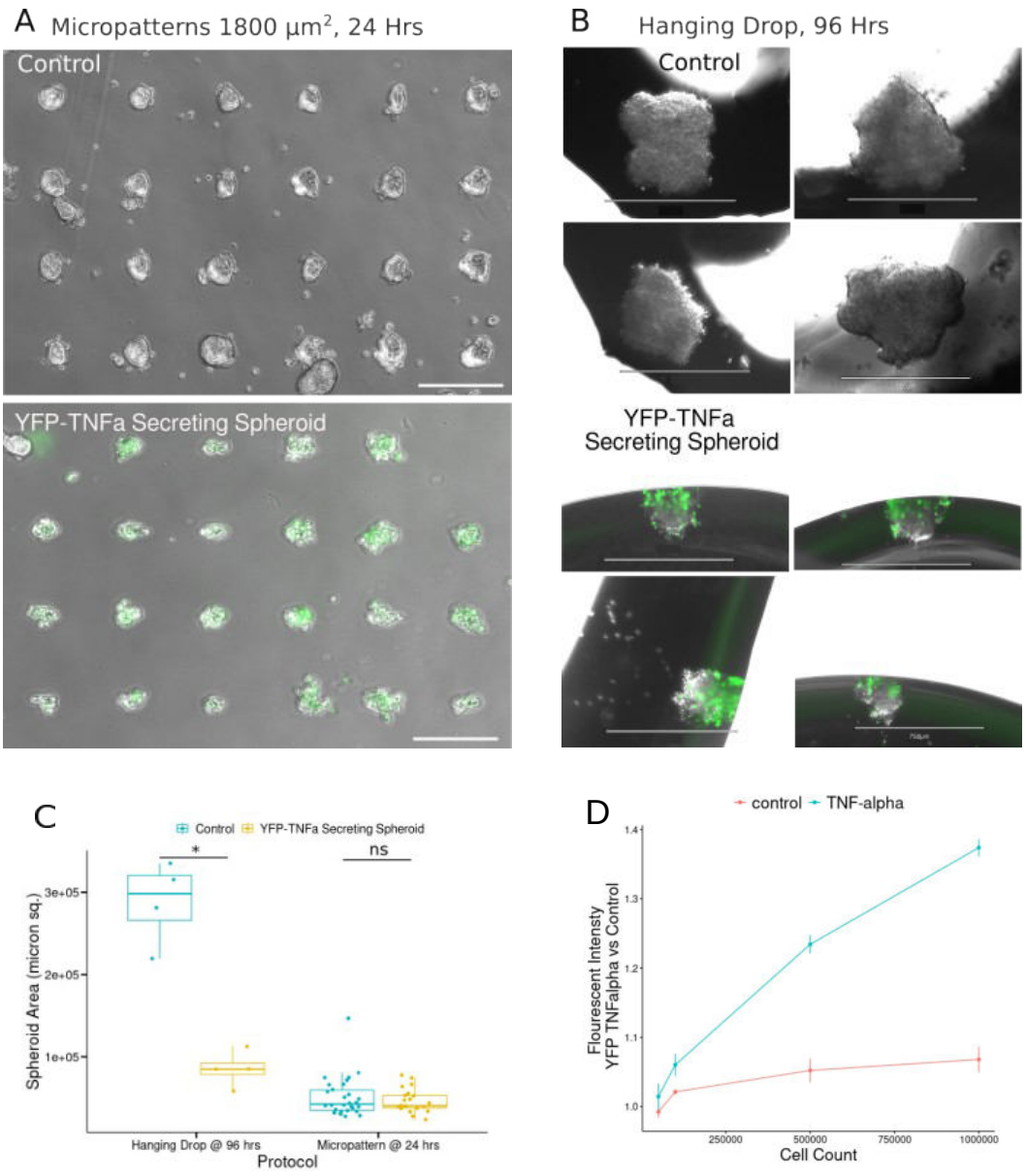

FIG. S1. Heterologous protein expression assay development. (**a**) Bright-field images of HEK293 spheroids growing over fibronectin micropatterns overlayed with the wide-field fluorescent image for control and YFP-TNFα secreting spheroids. (**b**) Bright-field images of HEK293 spheroids growing in a droplet of cell culture media overlayed with wide-field fluorescent images for control and tumor-mimicking spheroids. (**c**) Box plot representing the projected area (sq μm) of spheroid grown on micropattern surface (n$\geq$20 spheroids) vs spheroids grown through hanging drop method (n=4 spheroids). (**d**) Fluorescence intensity of YFP emission signal from the collected conditioned media at different cell densities of YFP-TNFα transfected HEK cells against the control. n=3 per condition, p-value (ANOVA) $\leq$ 0.000207. Scale Bar (A) 500 μm (B) 750 μm. p-value (Wilcoxon rank-sum test) *: $\leq$ 0.05, ns: non significant.

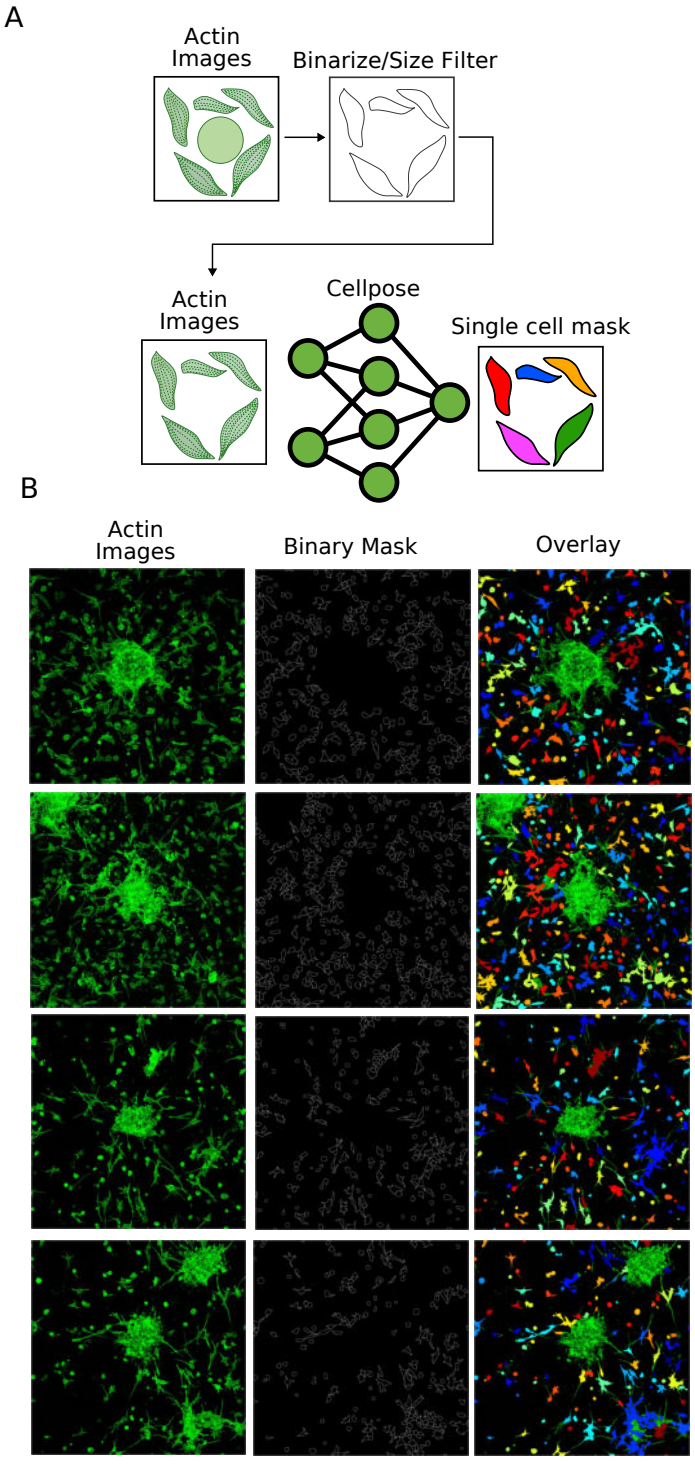

FIG. S2. Single cell image segmentation validation (**a**) The single-cell segmentation workflow from max Z projected Actin confocal images of fibroblasts-spheroid 3D co-culture. (**b**) Representative max-Z projected Actin confocal images showing, the corresponding binary mask, and overlay showing image segmentation performance.

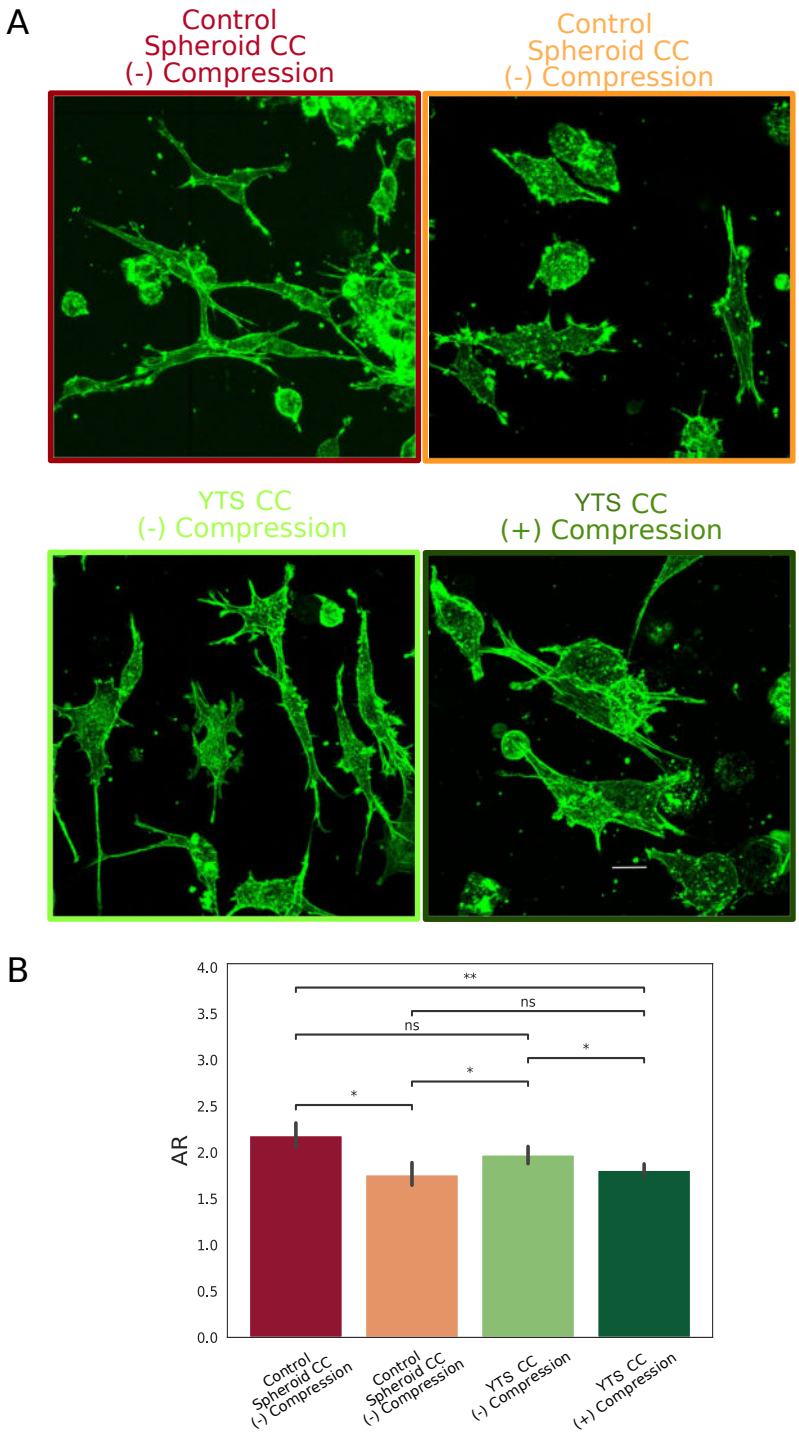

FIG. S3. Actin depolymerization under Compressive Forces and TNFα (**a**) Max Z projected actin confocal images of fibroblasts under the perturbation condition. (**b**) Bar plot showing the Aspect Ratio of fibroblasts under different perturbation conditions. n$\geq$400 cells per condition. p values (Wilcoxon rank-sum test): **** ≤ 0.0001, *** ≤ 0.001, ** ≤ 0.01, * ≤ 0.05)

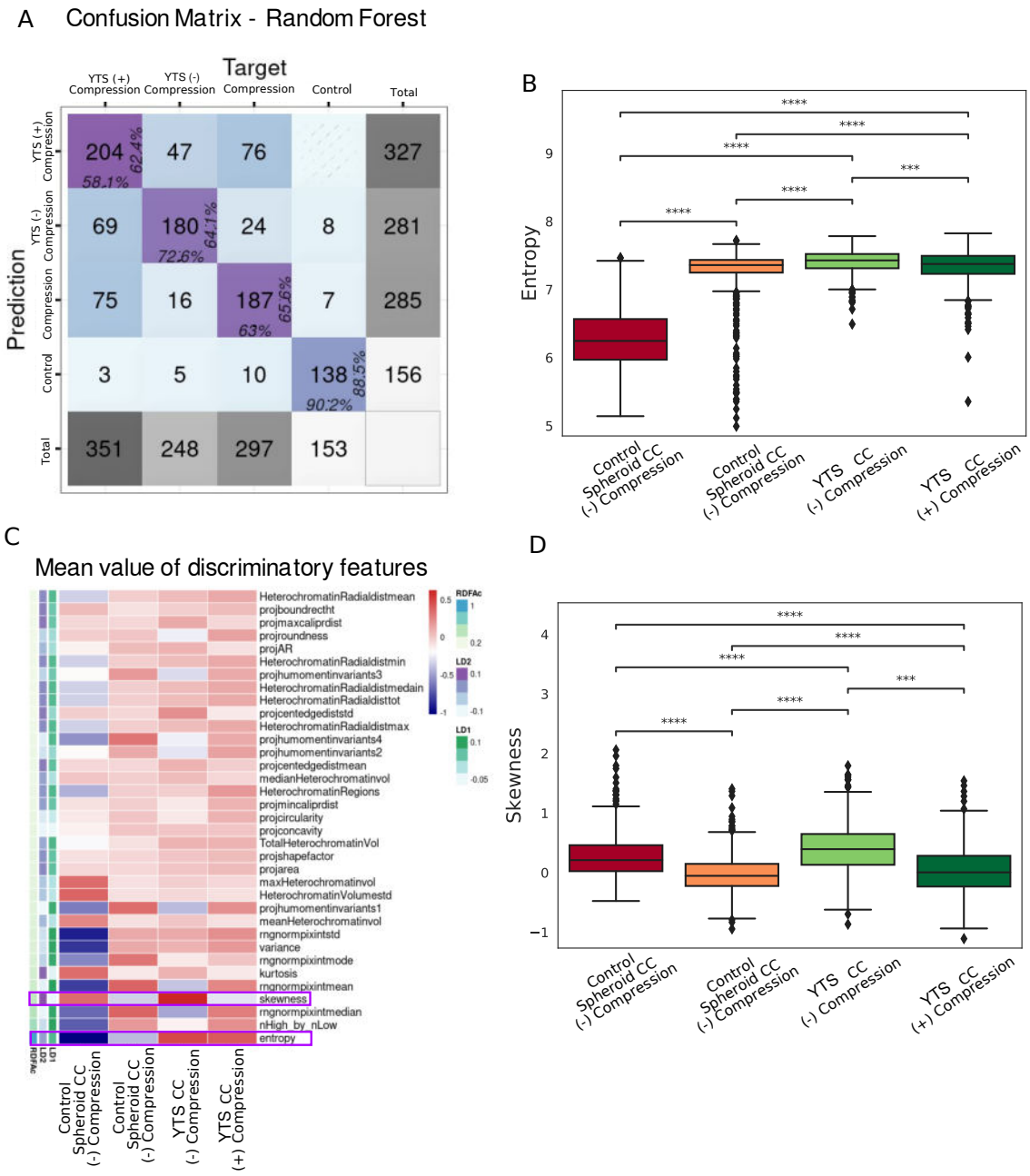

FIG. S4. Chromatin states under different perturbations (**a**) Confusion Matrix of Random Forest classification. (**b**) Box plot showing the Entropy of chromatin images under different perturbation conditions. (**c**) Heatmap showing the mean value of chromatin features sorted by their Random Forest Accuracy Score (RFAc). Further annotation to the heatmap represents, the corresponding LD1 (linear discriminatory) and LD2 coefficient corresponding to a particular feature (**d**) Box plot showing the Skewness of chromatin images under different perturbation conditions. (p values (Wilcoxon rank-sum test): **** $\leq$ 0.0001, *** $\leq$ 0.001, ** $\leq$ 0.01, * $\leq$ 0.05). n$\geq$400 cells per condition.

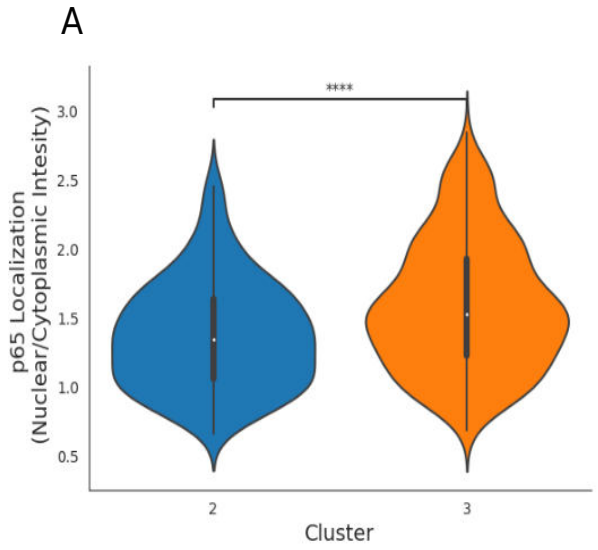

FIG. S5. (A) Violin plot showing the relative p65 localization (Nuclear Intensity/Cytoplasmic Intensity) for HMF3A cells cocultured with tumor-mimicking spheroids under compression clustered in different respective clusters via FNN. p values (Wilcoxon rank-sum test): **** ≤ 0.0001, *** ≤ 0.001, ** ≤ 0.01, * ≤ 0.05, n$\geq$100 cells per condition.

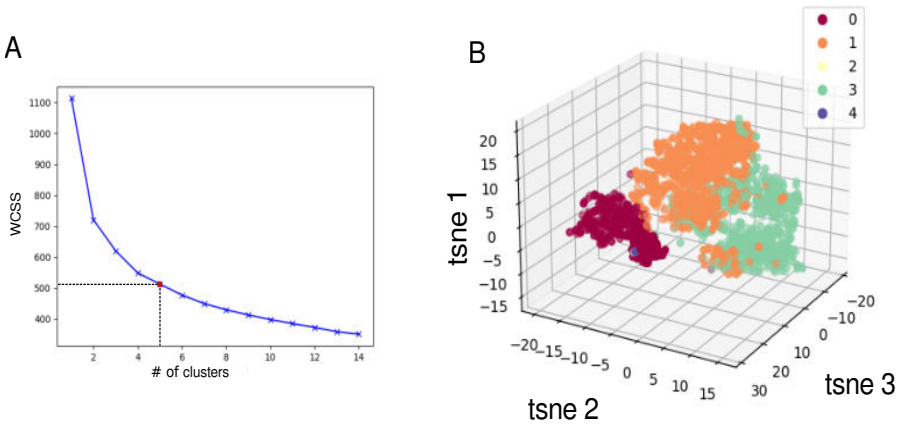

FIG. S6. (A) Elbow plot of WCSS after K-Means clustering with # of input clusters. (B) RAW clustering was obtained by choosing n=5 as an optimal number of clusters.

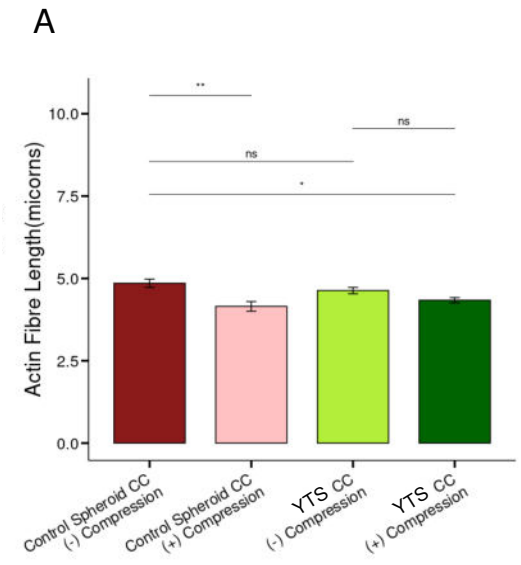

FIG. S7. (A) Mean actin fiber segment length for each condition, the error bar represents the mean standard error. p values (Wilcoxon rank-sum test): **** ≤ 0.0001, *** ≤ 0.001, ** ≤ 0.01, * ≤ 0.05, n$\geq$400 cells per condition.

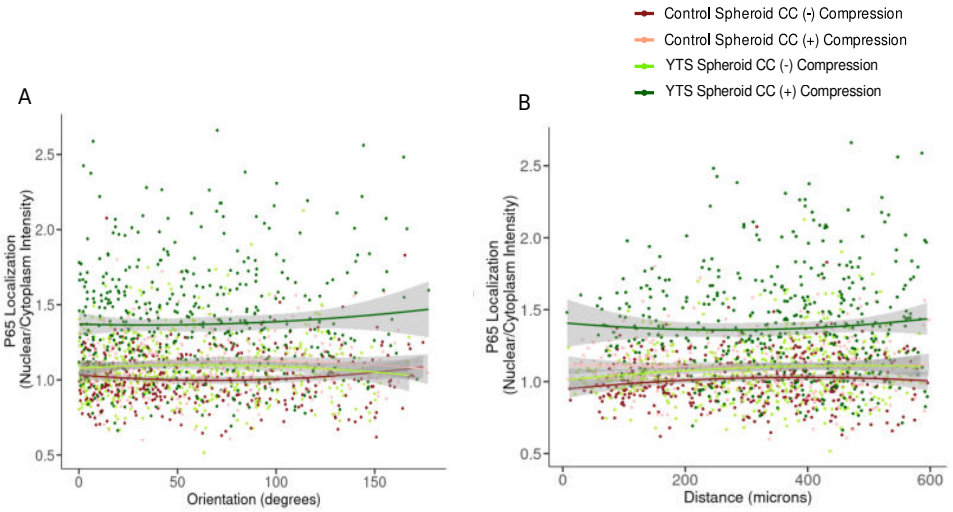

FIG. S8. (A) Orientation of the cell, the angle measured between the cell major axis and the radial axis passing through the spheroid centroid (B) Radial distance between the cell centroid from the spheroid centroid for Control Spheroid CC(-) Compression, Control Spheroid CC(+) Compression, YTS Spheroid (-) Compression, YTS Spheroid (+) Compression.

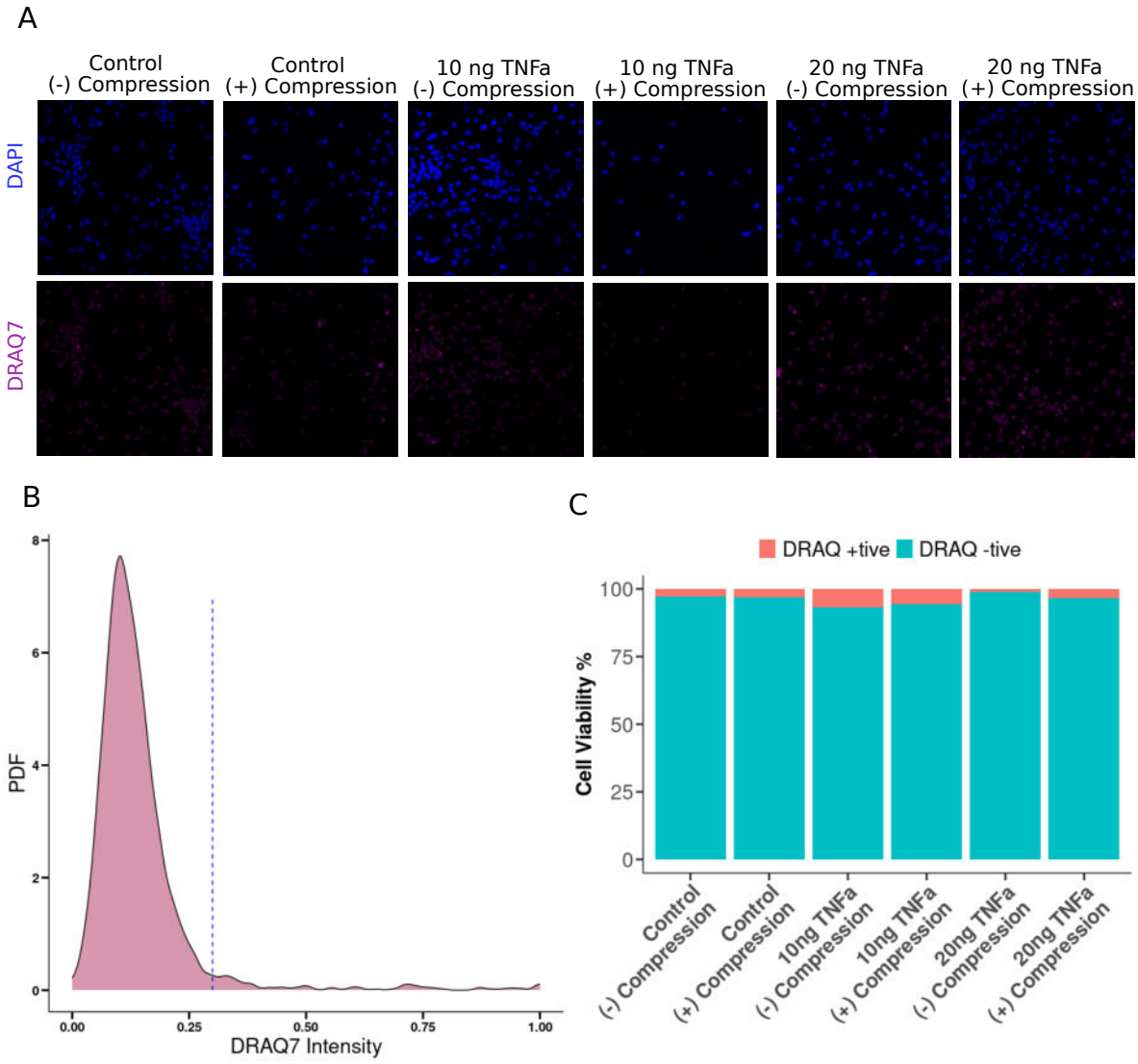

FIG. S9. (A) Representative images of nuclear staining with DRAQ7 representing cell viability (B) Normalized intensity histogram of DRAQ7 staining, blue annotation representing the threshold of cell viability. (C) Stacked bar plot representing cell viability percentages with varying concentrations of TNFα and compression, n$\geq$200 cells per condition.

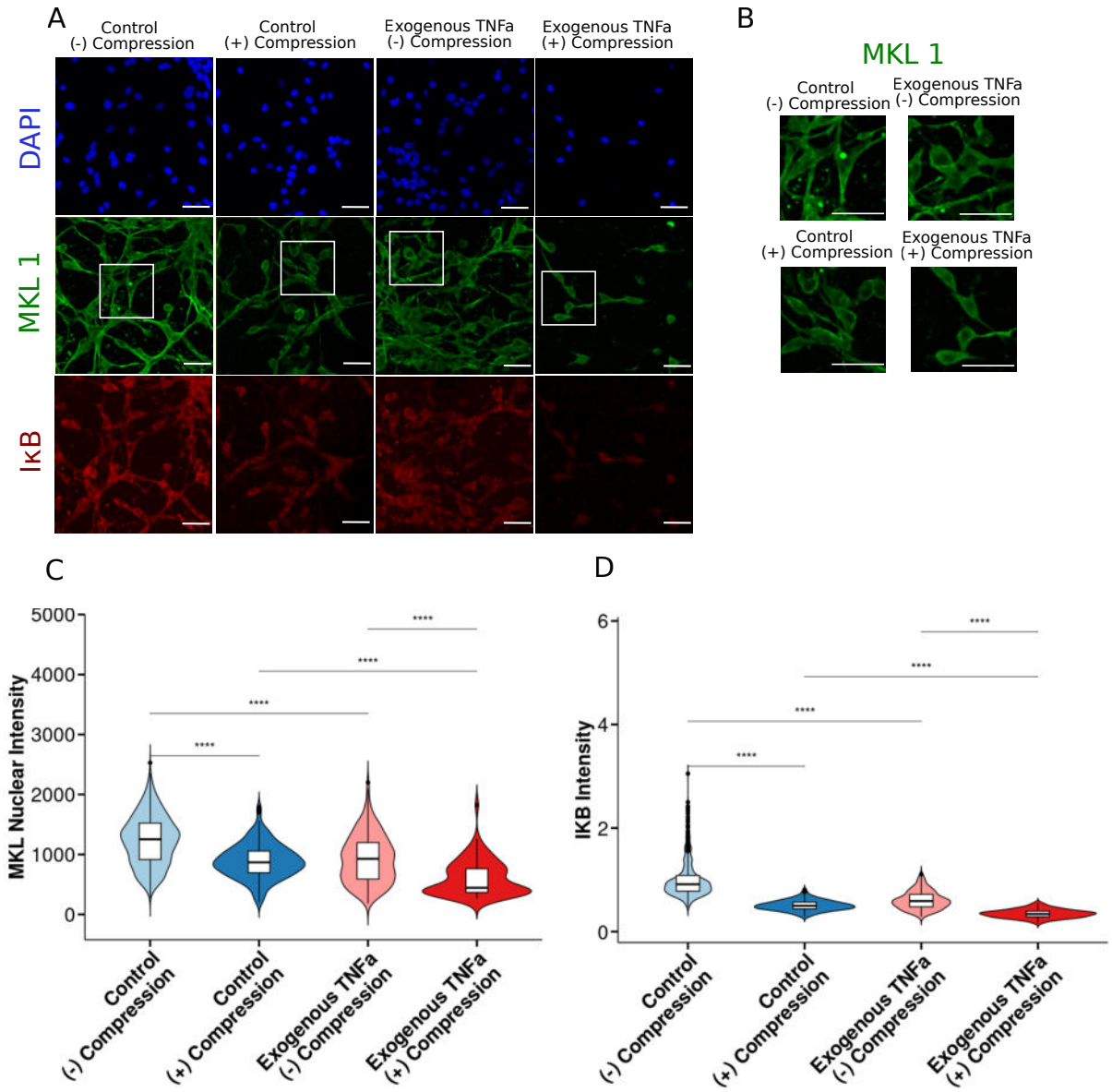

FIG. S10. (A)&(B) Representative fluorescence images of MKL 1 (green), IκB (red), and nuclei (blue) for HMF3A cells treated with exogenous TNFα. The region of images showing MKL 1 localization highlighted with a white boundary has been enlarged highlighting the difference in MKL 1 nuclear localization. Images are shown for HMF3A cells embedded in collagen matrix with and without compression as control (left two columns), and HMF3A cells embedded in collagen matrix and treated with exogenous TNFα with and without compression (right two columns). (C) Boxplot showing the MKL 1 nuclear localization for the HMF3A cells in each of the conditions. p value (ANOVA) $\leq$ 0.000263 (D) Boxplot showing the relative IκB intensity of the HMF3A cells in each of the conditions, p value (ANOVA) $\leq$ 3.18e-07. Scalebar: 25μm, p values (Wilcoxon rank-sum test): **** $\leq$ 0.0001, *** $\leq$ 0.001, ** $\leq$ 0.01, * $\leq$ 0.05, n$\geq$400 cells per condition.

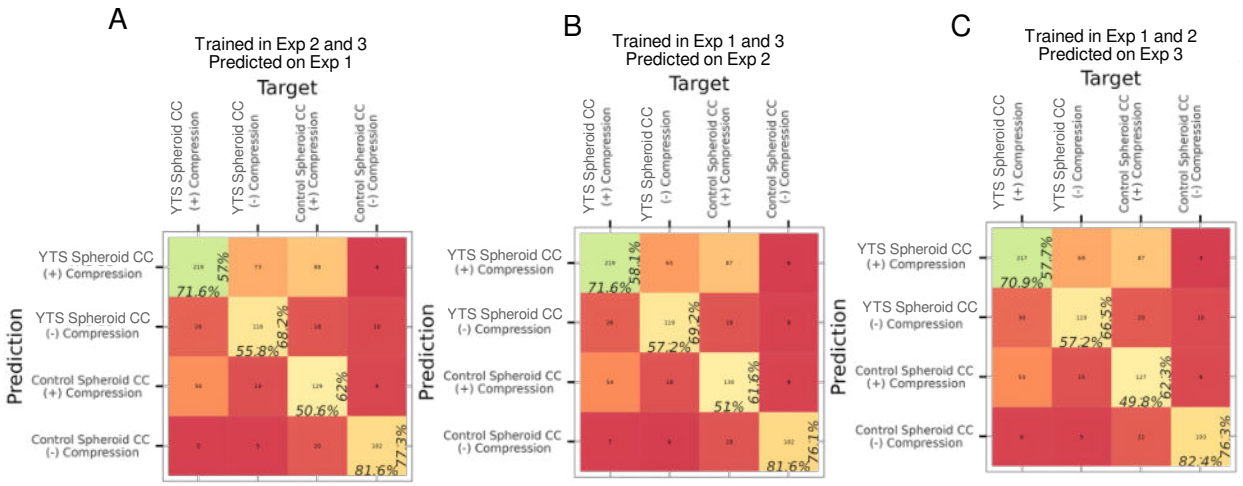

FIG. S11. (A) Confusion Matrix obtained from choosing training data from Experimental Batch 2&3 and testing data as Experimental Batch 1, (B) Confusion Matrix obtained from choosing training data as Experimental Batch 1&3 and testing data as Experimental Batch 2, (C) Confusion Matrix obtained from choosing training data as Experimental Batch 1&2 and testing data as Experimental Batch 3.